Mineralogical Magazine (2023), **87**, 178–185
doi:10.1180/mgm.2022.132

CAMBRIDGE UNIVERSITY PRESS

Article

Crystal chemistry of povondraite by single-crystal XRD, EMPA, Mössbauer spectroscopy and FTIR

Ferdinando Bosi[1]*, Henrik Skogby[2] and Guy L. Hovis[3]

[1]Department of Earth Sciences, Sapienza University of Rome, Piazzale A. Moro, 5, I-00185 Rome, Italy; [2]Department of Geosciences, Swedish Museum of Natural History, Box 50007, SE-10405 Stockholm, Sweden and [3] Department of Geology and Environmental Geosciences, Lafayette College, Easton, PA 18042, Pennsylvania, USA

Abstract

Five povondraite crystals from San Francisco Mine, Villa Tunari, Bolivia, have been structurally and chemically characterised by single-crystal X-ray diffraction and electron microprobe analysis. For the first time, this characterisation is accompanied by Mössbauer spectroscopic and single-crystal infrared spectroscopic data, which show the exclusive presence of Fe^{3+} at both the octahedrally-coordinated *Y* and *Z* sites as well as slight disorder of (OH) and O over the O(1) and O(3) sites.

The data obtained along with those for earlier-studied bosiite and oxy-dravite oxy-tourmalines show a complete substitution series described by the reaction ${}^{Y}Fe_3^{3+} + {}^{Z}Mg + {}^{Z}Fe_4^{3+} \leftrightarrow {}^{Y}Al_2 + {}^{Y}Mg + {}^{Z}Al_5$ (i.e. $Fe^{3+}Al_{-1}$) with variation of the structural parameters dominated by Fe^{3+} (or Al). Povondraite is the tourmaline member having the largest unit-cell parameters due to the larger size of Fe^{3+} relative to other trivalent cations (V > Cr > Al). In the tourmaline-supergroup minerals, the *a* and *c* unit-cell parameters vary from ~15.60 Å to ~16.25 Å and ~7.00 Å to ~7.50 Å, respectively. Their values increase with increasing Fe^{3+} or decreasing Al. End-member compositions related to the smallest and largest *a* and *c* parameters are, respectively, $NaAl_3Al_6(Si_3B_3O_{18})(BO_3)_3(OH)_3(OH)$ (synthetic tourmaline) and $NaFe_3^{3+}(Fe_4^{3+}Mg_2)(Si_6O_{18})(BO_3)_3(OH)_3O$ (povondraite).

Keywords: povondraite, crystal-structure refinement, electron microprobe, Mössbauer spectroscopy, infrared spectroscopy, crystal chemistry

(Received 5 September 2022; accepted 20 November 2022; Accepted Manuscript published online: 28 November 2022; Associate Editor: Charles A. Geiger)

Introduction

Tourmalines are complex borosilicates whose general chemical formula may be written as: $XY_3Z_6T_6O_{18}(BO_3)_3V_3W$, where X = Na^+, K^+, Ca^{2+} and ▫ (= vacancy); Y = Al^{3+}, Fe^{3+}, Cr^{3+}, V^{3+}, Mg^{2+}, Fe^{2+}, Mn^{2+} and Li^+; Z = Al^{3+}, Fe^{3+}, Cr^{3+}, V^{3+}, Mg^{2+} and Fe^{2+}; T = Si^{4+} Al^{3+} and B^{3+}; B = B^{3+}; V = $(OH)^-$ and O^{2-}; W = $(OH)^-$, F^- and O^{2-} (Henry *et al.*, 2011). In this representation unitalicised letters X, Y, Z, T and B represent groups of cations hosted at the ${}^{[9]}X$, ${}^{[6]}Y$, ${}^{[6]}Z$, ${}^{[4]}T$ and ${}^{[3]}B$ crystallographic sites (letters italicised), whereas V and W represent groups of anions accommodated at the [3]-coordinated O(3) and O(1) crystallographic sites, respectively.

Tourmaline has been studied extensively in terms of crystal structure and crystal chemistry (e.g. Foit, 1989; Grice and Ercit, 1993; Hawthorne and Henry, 1999; Ertl *et al.*, 2002; Novák *et al.*, 2004; Bosi and Lucchesi, 2007; Bosi, 2018; Henry and Dutrow, 2011; Henry *et al.*, 2011; Cempírek *et al.*, 2013; Bačík and Fridrichová, 2020). Results show that the tourmaline structure is remarkably flexible in a chemical sense, accommodating ions of a wide range of size and charge, which in turn leads to Mg–Fe–Al–Cr–V disorder over the *Y* and *Z* sites.

Povondraite, ideally $NaFe_3^{3+}(Fe_4^{3+}Mg_2)(Si_6O_{18})(BO_3)_3(OH)_3O$, was described by Grice *et al.* (1993). Until now, however, a chemical and structural study dealing with a statistically significant dataset of Fe^{3+}-dominant oxy-tourmalines is missing. To explore the crystal-chemical aspects and their implications on the tourmaline supergroup, single-crystal structure refinements and electron microprobe data have been collected on five crystals from the type locality for povondraite: San Francisco Mine, Villa Tunari, Alto Chapare, Cochabamba, Bolivia (Walenta and Dunn, 1979; Grice *et al.*, 1993; Žáček *et al.*, 2000). All five single crystals were extracted from povondraite sample 110379 from the American Museum of Natural History, New York, USA. This is the first time that Mössbauer spectroscopic and single-crystal infrared spectroscopic data have been presented for this mineral.

Analytical methods and results

General comment

Initially, several crystal fragments of sample 110379 were analysed by electron microprobe; these proved to be chemically inhomogeneous, as reported in Hovis *et al.* (in press). More recent analyses, reported in the present study, were obtained on different

*Author for correspondence: Ferdinando Bosi, Email: ferdinando.bosi@uniroma1.it
Cite this article: Bosi F., Skogby H. and Hovis G.L. (2023) Crystal chemistry of povondraite by single-crystal XRD, EMPA, Mössbauer spectroscopy and FTIR. *Mineralogical Magazine* **87**, 178–185. https://doi.org/10.1180/mgm.2022.132

© The Author(s), 2022. Published by Cambridge University Press on behalf of The Mineralogical Society of Great Britain and Ireland. This is an Open Access article, distributed under the terms of the Creative Commons Attribution licence (http://creativecommons.org/licenses/by/4.0/), which permits unrestricted re-use, distribution and reproduction, provided the original article is properly cited.

Table 1. Single-crystal X-ray diffraction data details for the povondraite crystals studied.*

	Pov1	Pov4	Pov3	Pov2	Pov5
Crystal size (mm)	0.06 × 0.08 × 0.10	0.12 × 0.16 × 0.22	0.22 × 0.26 × 0.36	0.20 × 0.22 × 0.25	0.07 × 0.12 × 0.16
a (Å)	16.1679(2)	16.2095(5)	16.2165(4)	16.2308(3)	16.2366(3)
c	7.4122(1)	7.4499(3)	7.4609(4)	7.4676(1)	7.4688(2)
V (Å^3)	1677.97(5)	1695.20(12)	1699.17(12)	1703.69(7)	1705.19(8)
Reciprocal space range hkl	$-23 \le h \le 26$ $-27 \le k \le 27$ $-12 \le l \le 11$	$-27 \le h \le 23$ $-26 \le k \le 27$ $-11 \le l \le 12$	$-27 \le h \le 26$ $-27 \le k \le 27$ $-10 \le l \le 10$	$-27 \le h \le 26$ $-22 \le k \le 27$ $-12 \le l \le 12$	$-27 \le h \le 26$ $-22 \le k \le 27$ $-12 \le l \le 12$
Set of read reflections	12,604	11,847	7063	12,144	12,409
Unique reflections, R_{int} (%)	1943, 4.46	1996, 3.80	1704, 3.46	2067, 2.59	2088, 3.32
Unique reflections with $I > 2\sigma I$	1803	1926	1547	2028	1996
Redundancy	12	11	6	11	11
Restraints, refined parameters	1, 94	1, 94	1, 94	1, 94	1, 94
Flack parameter	0.060(16)	0.006(14)	0.03(2)	0.021(10)	0.008(13)
wR_2 (%)	3.45	4.14	5.90	2.83	3.66
R_1 (%) all data	2.72	2.16	3.61	1.53	2.22
R_1 (%) for $I > 2\sigma_I$	2.21	1.94	2.68	1.47	2.01
GoF	1.017	1.020	1.095	1.062	1.054
Largest diff. peak and hole (e^-/Å^3)	0.58 and −0.58	1.04 and −0.53	0.97 and −0.74	0.74 and −0.65	1.03 and −1.00

*Notes: R_{int} = merging residual value; R_1 = discrepancy index, calculated from F-data; wR_2 = weighted discrepancy index, calculated from F^2-data; GoF = goodness of fit; diff. peak = maximum and minimum residual electron density. Space-group type = $R3m$ and $Z = 3$. Radiation: Mo$K\alpha$ = 0.71073 Å. Range for data collection (2θ) = 5°–75°. Data collection temperature = 293 K. Axis = phi-omega, frame width = 0.4°, time per frame = 20 s. Absorption correction method: multi-scan (*SADABS*, Bruker). Refinement method: full-matrix last-squares on F^2. Structural refinement program: *SHELXL-2013* (Sheldrick, 2015).

relatively small fragments, which proved to be quite homogeneous as shown by the relatively low standard deviation values of the analysed elements (Table 4).

Single-crystal structure refinement (SREF)

Single-crystal X-ray diffraction (XRD) was undertaken on five crystal fragments of povondraite by mounting on a Bruker KAPPA APEX-II single-crystal diffractometer (Sapienza University of Rome, Earth Sciences Department) equipped with a CCD area detector (6.2 × 6.2 cm active detection area, 512 × 512 pixels) and a graphite-crystal monochromator using Mo$K\alpha$ radiation from a fine-focus sealed X-ray tube. The sample-to-detector distance was 4 cm. A total of 1296 exposures (step = 0.4° and time/step = 20 s) covering a full reciprocal sphere were collected using ω and φ scan modes. Final unit-cell parameters were refined using the Bruker AXS *SAINT* program on reflections with $I > 10\ \sigma_I$ in the range 5° < 2θ < 75°. The intensity data were processed and corrected for Lorentz polarisation and background effects using the *APEX2* software program of Bruker AXS. The data were corrected for absorption using a multi-scan method (*SADABS*). The absorption correction led to an improvement in R_{int}. No violation of $R3m$ symmetry was detected.

Structure refinement was done using the *SHELXL-2013* program (Sheldrick, 2015). Starting coordinates were taken from Grice *et al.* (1993). Variable parameters included scale factor, extinction coefficient, atom coordinates, site-scattering values (for X, Y and Z sites) and atomic-displacement factors. Each structure was refined as a two-component inversion twin. Fully ionised-oxygen scattering factor and neutral-cation scattering factors were used. In detail, the X site was modelled using the Na *vs.* K scattering factors. The occupancy of the Y site was obtained by considering the presence of Fe *vs.* Mg, and the Z site with Fe *vs.* Al. Although there is more Mg than Al content, the latter was preferred to ^{Z}Mg, having produced slightly better statistical indices and standard uncertainties. The T, B and anion sites were modelled, respectively, with Si, B and O scattering factors and with a fixed occupancy of 1, as refinement with unconstrained occupancies showed no significant deviations from this value. The position of the H atom bonded to the oxygen at the O(3) site in the structure was taken from the difference-Fourier map and incorporated into the refinement model; the O(3)–H(3) bond length was restrained (by DFIX command) to be 0.97 Å with isotropic displacement parameter constrained to be equal to 1.2 times that obtained for the O(3) site. Table 1 lists crystal data, data-collection information, and refinement details. Table 2 gives the fractional atom coordinates and equivalent isotropic-displacement parameters of a typical povondraite crystal (Pov1). Table 3 reports selected bond lengths for all studied crystals. The crystallographic information files showing all structural data have been deposited with the Principal Editor of *Mineralogical Magazine* and are available as Supplementary material (see below).

Electron microprobe analysis (EMPA)

The crystals used for X-ray diffraction refinement were analysed by wavelength dispersive spectrometry (WDS mode) using a Cameca SX50 instrument (CNR-Istituto di Geologia Ambientale e Geoingegneria, Rome, Italy) operating at an accelerating potential of 15 kV and a sample current of 15 nA, with a 10 μm beam diameter. The following standards, X-ray $K\alpha$ lines and analyser crystals were used: jadeite (Na; TAP), periclase (Mg; TAP), orthoclase (K; PET), rutile (Ti; PET), wollastonite (Si, Ca; PET), metallic Zn and Mn (Zn, Mn; LIF), vanadinite (V; PET), fluorophlogopite (F; TAP), metallic Cr (Cr; PET), corundum (Al; TAP) and magnetite (Fe; LIF). The 'PAP' routine was applied (Pouchou and Pichoir 1991). The results (Table 4) represent mean values of several spot analyses. Vanadium, Cr, Mn and Zn were below detection limits (< 0.03 wt.%).

Mössbauer spectroscopy

Several crystal fragments from povondraite sample 110379 were used for ^{57}Fe Mössbauer spectroscopy performed at the Swedish

https://doi.org/10.1180/mgm.2022.132 Published online by Cambridge University Press

Table 2. Fractional atom coordinates and isotropic (*) or equivalent-isotropic displacement parameters (in Å^2) for crystal Pov1.

	x	*y*	*z*	$U_{eq/iso}$
X	0	0	0.2301(3)	0.0254(9)
Y	0.12289(3)	0.06144(2)	0.64141(11)	0.00678(14)
Z	0.29863(3)	0.26242(3)	0.61228(10)	0.00570(9)
B	0.10972(12)	0.2194(2)	0.4571(5)	0.0065(5)
T	0.18983(3)	0.18824(4)	0	0.00464(12)
O(1)	0	0	0.7713(6)	0.0098(7)
O(2)	0.06115(7)	0.12229(14)	0.4885(3)	0.0069(4)
O(3)	0.25938(16)	0.12969(8)	0.5118(3)	0.0102(4)
H(3)	0.259(3)	0.1297(13)	0.381(3)	0.012*
O(4)	0.09230(7)	0.18460(15)	0.0689(3)	0.0086(4)
O(5)	0.18267(15)	0.09134(8)	0.0864(3)	0.0088(4)
O(6)	0.19327(10)	0.18412(10)	0.7834(2)	0.0071(3)
O(7)	0.28184(9)	0.28175(9)	0.0761(2)	0.0074(3)
O(8)	0.20682(10)	0.26785(10)	0.4411(2)	0.0096(3)

*Isotropic-displacement parameters (U_{iso}) for H(3) constrained to have a U_{iso} 1.2 times the U_{eq} value of the O(3) oxygen atom, respectively.

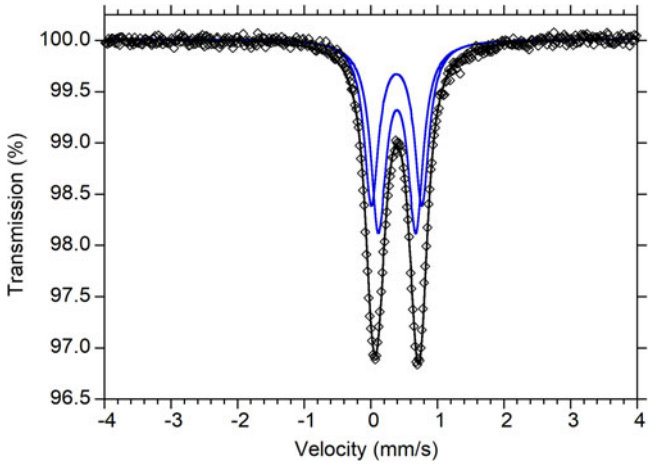

Fig. 1. Mössbauer spectrum of povondraite obtained at room temperature. The fitted absorption doublets assigned to Fe^{3+} are indicated in blue. Diamonds denote the measured spectrum and the black curve represents summed fitted doublets.

Museum of Natural History, Stockholm, Sweden, using a conventional spectrometer system operated in constant-acceleration mode. Data were collected over 1024 channels; these were folded and calibrated against the spectrum of α-Fe foil. The spectrum (Fig. 1) was fit using the software *MossA* (Prescher *et al.*, 2012) with two absorption doublets consistent with Fe^{3+} (Table 5). No indications of absorption due to Fe^{2+} was observed. In line with the site population results from SREF (see below, Table 6), the two doublets can be related to the occurrence of Fe^{3+} at both the *Y* and *Z* sites. However, the low resolution of the two doublets does not allow a definite site assignment.

The Mössbauer spectroscopy results are consistent with a synchrotron XANES study that reported 87–100% Fe as Fe^{3+} (Levy *et al.*, 2018).

Table 3. Selected bond lengths (Å) and cation site occupancy (s.o.) for the povondraite crystals studied.*

	Pov1	Pov4	Pov3	Pov2	Pov5
X–O(2) ×3	2.570(3)	2.588(3)	2.592(5)	2.614(2)	2.605(3)
X–O(5) ×3	2.771(2)	2.768(2)	2.768(4)	2.7707(16)	2.771(2)
X–O(4) ×3	2.847(2)	2.848(2)	2.846(4)	2.8458(17)	2.850(2)
<*X*–O>	2.729	2.735	2.735	2.744	2.742
s.o.(*X*)	$Na_{0.824(18)}$ $K_{0.176(18)}$	$Na_{0.85(2)}$ $K_{0.15(2)}$	$Na_{0.90(3)}$ $K_{0.10(3)}$	$Na_{0.767(15)}$ $K_{0.233(15)}$	$Na_{0.78(2)}$ $K_{0.22(2)}$
Y–O(1)	1.972(2)	1.9653(19)	1.966(4)	1.9645(13)	1.9644(18)
Y–O(6) ×2	2.0200(15)	2.0180(15)	2.019(3)	2.0182(11)	2.0195(15)
Y–O(2) ×2	2.0568(15)	2.0608(14)	2.063(3)	2.0611(10)	2.0618(14)
Y–O(3)	2.139(2)	2.138(2)	2.138(4)	2.1368(17)	2.139(2)
<*Y*–O>	2.044	2.043	2.045	2.043	2.044
s.o.(*Y*)	$Fe_{0.773(5)}$ $Mg_{0.227(5)}$	$Fe_{0.857(7)}$ $Mg_{0.143(7)}$	$Fe_{0.866(10)}$ $Mg_{0.134(10)}$	$Fe_{0.888(4)}$ $Mg_{0.112(4)}$	$Fe_{0.908(6)}$ $Mg_{0.0.92(5)}$
Z–O(8)	1.9583(15)	1.9699(14)	1.971(2)	1. 9731(11)	1.9749(14)
Z–O(7)	1.9810(15)	1.9930(15)	1.993(3)	2.0002(11)	2.0019(15)
Z–O(8)’	1.9877(15)	1.9962(15)	1.994(3)	2.0016(11)	2.0021(14)
Z–O(6)	1.9893(15)	2.0084(15)	2.015(3)	2.0176(11)	2.0196(15)
Z–O(7)’	2.0143(14)	2.0262(14)	2.031(2)	2.0311(10)	2.0325(14)
Z–O(3)	2.0496(11)	2.0644(11)	2.068(2)	2.0711(8)	2.0725(10)
<*Z*–O>	1.997	2.010	2.012	2.016	2.017
s.o.(*Z*)	$Fe_{0.513(4)}$ $Al_{0.487(4)}$	$Fe_{0.639(5)}$ $Al_{0.361(5)}$	$Fe_{0.657(8)}$ $Al_{0.343(8)}$	$Fe_{0.687(4)}$ $Al_{0.313(4)}$	$Fe_{0.713(5)}$ $Al_{0.287(5)}$
B–O(8) ×2	1.365(2)	1.366(2)	1.371(3)	1.3662(15)	1.366(2)
B–O(2)	1.380(4)	1.385(3)	1.383(6)	1.387(3)	1.389(4)
<*B*–O>	1.370	1.372	1.375	1.373	1.374
T–O(7)	1.6023(14)	1.6042(13)	1.607(2)	1.6043(10)	1.6047(14)
T–O(6)	1.6087(17)	1.6141(18)	1.615(3)	1.6140(12)	1.6142(16)
T–O(4)	1.6302(9)	1.6307(9)	1.6330(16)	1.6307(6)	1.6316(9)
T–O(5)	1.6423(10)	1.6445(10)	1.6454(19)	1.6425(7)	1.6438(9)
<*T*–O>	1.621	1.623	1.625	1.623	1.624

*Note: *T*-site occupancy = $Si_{1.00}$ and B-site occupancy = $B_{1.00}$

Table 4. Chemical composition for the povondraite crystals studied.*

	Pov1 (4 spots)	Pov4 (5 spots)	Pov3 (5 spots)	Pov2 (8 spots)	Pov5 (9 spots)
SiO_2 (wt.%)	31.56(33)	30.52(23)	30.19(18)	30.00(29)	29.80(35)
TiO_2	0.52(69)	b.d.l.	b.d.l.	b.d.l.	b.d.l.
B_2O_3[a]	9.20	8.92	8.98	8.80	8.77
Al_2O_3	6.75(71)	3.25(62)	2.75(34)	1.74(51)	0.76(30)
Fe_2O_3[b]	38.25(76)	43.96(58)	45.40(31)	45.95(20)	47.41(39)
MgO	7.17(81)	6.41(44)	6.66(21)	6.28(33)	6.24(27)
CaO	0.04(3)	b.d.l.	b.d.l.	b.d.l.	b.d.l.
Na_2O	2.44(12)	2.16(14)	2.26(9)	2.07(12)	2.03(12)
K_2O	0.51(8)	0.83(16)	0.68(12)	0.92(14)	0.95(12)
F	b.d.l.	b.d.l.	0.03(4)	b.d.l.	b.d.l.
H_2O[a]	2.34	2.23	2.36	2.20	2.21
O=F	-	-	−0.01	-	-
Total	98.78	98.28	99.30	97.97	98.16
Si (apfu)	5.96	5.95	5.84	5.92	5.91
Ti	0.07	-	-	-	-
B	3.00	3.00	3.00	3.00	3.00
Al	1.50	0.75	0.63	0.40	0.18
Fe^{3+}	5.44	6.45	6.61	6.83	7.07
Mg	2.02	1.86	1.92	1.85	1.84
Ca	0.01	-	-	-	-
Na	0.89	0.81	0.85	0.79	0.78
K	0.12	0.21	0.17	0.23	0.24
F	-	-	0.02	-	-
(OH)	2.95	2.90	3.04	2.90	2.92

*Notes: wt.% = weighted percent; apfu = atoms per formula unit (normalised to 31 anions); epfu = electrons per formula unit; b.d.l. = below detection limit; errors for oxides and fluorine are standard deviations (in brackets).
[a]Calculated by stoichiometry, (Y+Z+T) = 15.00 apfu.
[b]Fe oxidation state determined by Mössbauer spectroscopy.

https://doi.org/10.1180/mgm.2022.132 Published online by Cambridge University Press

Table 5. Mössbauer parameters for povondraite obtained at room temperature.*

δ (mm/s)	ΔE_Q (mm/s)	FWHM (mm/s)	Area (%)	Assignment
0.38(1)	0.76(3)	0.26(2)	46(13)	$^{VI}Fe^{2+}$
0.39(1)	0.56(3)	0.27(2)	54(13)	$^{VI}Fe^{2+}$

*δ = centre shift, ΔE_Q = quadrupole splitting, FWHM = full width at half-maximum.

Single-crystal infrared spectroscopy

Polarised Fourier-transform infrared (FTIR) absorption spectra were measured on a 33 μm thick doubly polished single-crystal section oriented parallel to the **c**-axis. A Bruker Vertex spectrometer attached to a Hyperion 2000 microscope and equipped with a halogen lamp source, CaF_2 beamsplitter, ZnSe wiregrid polariser and InSb detector was used to collect spectra in the range 2000–13000 cm^{-1} at a resolution of 4 cm^{-1}. Spectra recorded in polarised mode parallel to the crystallographic **c**-axis (**E**||**c**) show a weak band at 3440 cm^{-1}, a very intense band around 3550 cm^{-1}, a significant band at 3593 cm^{-1} and a weak band at 3699 cm^{-1} (Fig. 2). As observed typically for polarised tourmaline spectra in the (OH) range, the main band is off-scale for the **E**||**c** direction due to excessive absorption. Spectra obtained perpendicular to the **c**-axis show considerably weaker bands.

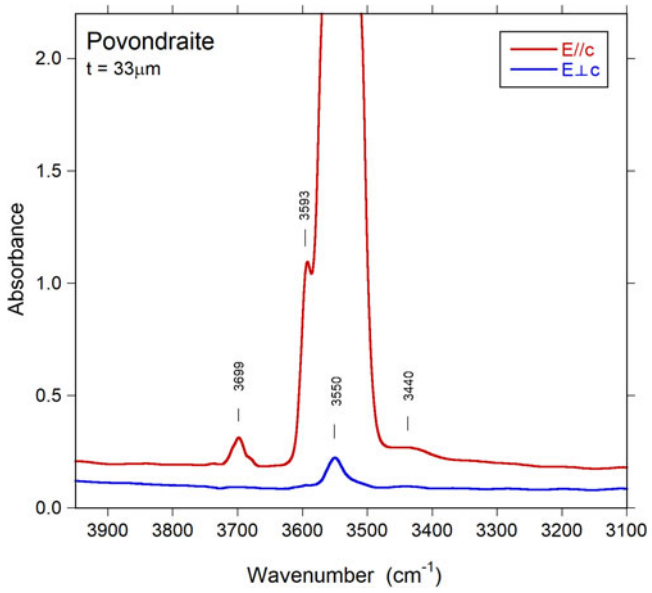

Fig. 2. Polarised FTIR spectra of povondraite, off-set vertically for clarity. The main band is truncated at ~2 absorbance units in the **E**||**c** direction due to excessive absorption. Note the comparatively low intensity of the band at ~3699 cm^{-1} corresponding to very small (OH) contents at W [≡ the O(1) site]. Sample thickness = 33 μm.

Table 6. Site populations (atoms per formula unit) and mean atomic number (man) for the povondraite crystals studied.*

	Pov1	Pov4	Pov3	Pov2	Pov5
***X* site**					
Na	0.89	0.81	0.85	0.79	0.78
K	0.12	0.21	0.17	0.23	0.24
Ca	0.01	-	-	-	-
Σ	1.03	1.02	1.02	1.03	1.02
$man_{(obs)}$	12.41(22)	12.20(24)	11.80(35)	12.86(19)	12.76(26)
$man_{(calc)}$	12.35	12.88	12.54	13.13	13.14
***Y* site**					
Fe^{3+}	2.26	2.54	2.56	2.64	2.69
Mg	0.66	0.46	0.44	0.36	0.31
Ti	0.07	-	-	-	-
Σ	3.00	3.00	3.00	3.00	3.00
$man_{(obs)}$	22.82(11)	24.00(17)	24.12(24)	24.43(10)	24.71(17)
$man_{(calc)}$	22.81	23.87	23.96	24.34	24.56
***Z* site**					
Fe^{3+}	3.18	3.90	4.05	4.18	4.38
Al	1.47	0.69	0.47	0.33	0.09
Mg	1.36	1.41	1.48	1.49	1.53
Σ	6.00	6.00	6.00	6.00	6.00
$man_{(obs)}$	19.67(8)	21.31(11)	21.54(17)	21.93(9)	22.27(11)
$man_{(calc)}$	19.66	21.22	21.52	21.81	22.24
***T* site**					
Si	5.96	5.95	5.84	5.92	5.91
Al	0.04	0.05	0.16	0.08	0.09
Σ	6.00	6.00	6.00	6.00	6.00
O(3) site					
OH	2.79	2.79	2.94	2.81	2.83
O	0.21	0.21	0.06	0.19	0.17
Σ	3.00	3.00	3.00	3.00	3.00
O(1) site					
OH	0.16	0.11	0.10	0.09	0.08
O	0.84	0.89	0.88	0.91	0.92
F	0.00	-	0.02	-	-
Σ	1.00	1.00	1.00	1.00	1.00

*Notes: All crystals have the *B* and O(2,4,5,6,7,8) sites fully occupied by B^{3+} and O^{2-}, respectively; obs = observed, calc = calculated from the site population.

Bands above 3600–3650 cm^{-1} are normally considered to be due to (OH) at the W position [≡ O(1) site] (e.g. Gonzalez-Carreño *et al.*, 1988; Bosi *et al.*, 2015). For the samples studied, the comparatively weak intensity of the band at 3699 cm^{-1} indicates low amounts of ^{W}(OH). On the basis of studies by Bosi *et al.* (2016), Watenphul *et al.* (2016) and Gatta *et al.* (2014), the main FTIR bands at ~3440 cm^{-1}, ~3550 and ~3593 cm^{-1} are probably caused by the occurrence of the atomic arrangements $3[^{Y}(Fe^{3+})^{Z}(Fe^{3+},Al)^{Z}(Al)]\text{–}^{O(3)}(OH)_3$, $\{2[^{Y}(Fe^{3+})^{Z}(Fe^{3+})^{Z}(Mg)]\text{–}[^{Y}(Fe^{3+})^{Z}(Fe^{3+})^{Z}(Fe^{3+})]\}\text{–}^{O(3)}(OH)_3$ and $3[^{Y}(Fe^{3+})^{Z}(Fe^{3+})^{Z}(Mg)]\text{–}^{O(3)}(OH)_3$, respectively,

Table 7. Weighted bond-valence sum (BVS, in valence units) and weighted atomic valence (WAV) calculated from site population for the povondraite crystals studied.*

Site	Pov1	Pov4	Pov3	Pov2	Pov5
$X_{(BVS)}$	0.93	0.98	0.94	0.98	0.99
$X_{(WAV)}$	1.03	1.02	1.02	1.03	1.02
$Y_{(BVS)}$	2.69	2.72	2.71	2.74	2.74
$Y_{(WAV)}$	2.81	2.85	2.85	2.88	2.90
$Z_{(BVS)}$	2.82	2.82	2.83	2.82	2.83
$Z_{(WAV)}$	2.77	2.77	2.75	2.75	2.74
$B_{(BVS)}$	3.02	3.00	2.98	2.99	2.99
$B_{(WAV)}$	3.00	3.00	3.00	3.00	3.00
$T_{(BVS)}$	4.04	4.01	3.99	4.02	4.01
$T_{(WAV)}$	3.99	3.99	3.97	3.99	3.98
$O(1)_{(BVS)}$	1.62	1.67	1.66	1.68	1.69
$O(1)_{(WAV)}$	1.84	1.89	1.88	1.91	1.92
$O(3)_{(BVS)}$	1.16	1.16	1.16	1.16	1.16
$O(3)_{(BVS)}$	1.07	1.07	1.02	1.06	1.06
$O(2)_{(BVS)}$	1.98	1.97	1.97	1.96	1.97
$O(4)_{(BVS)}$	1.16	1.16	1.16	1.16	1.16
$O(5)_{(BVS)}$	2.04	2.05	2.03	2.05	2.04
$O(6)_{(BVS)}$	2.00	1.99	1.99	2.01	2.00
$O(7)_{(BVS)}$	1.99	1.98	1.97	1.98	1.98
$O(8)_{(BVS)}$	2.00	1.99	1.99	1.99	1.99

*Note: The O(2,4,5,6,7,8) sites are fully occupied by O^{2-}. Bond valence parameters from Gagné and Hawthorne (2015).

https://doi.org/10.1180/mgm.2022.132 Published online by Cambridge University Press

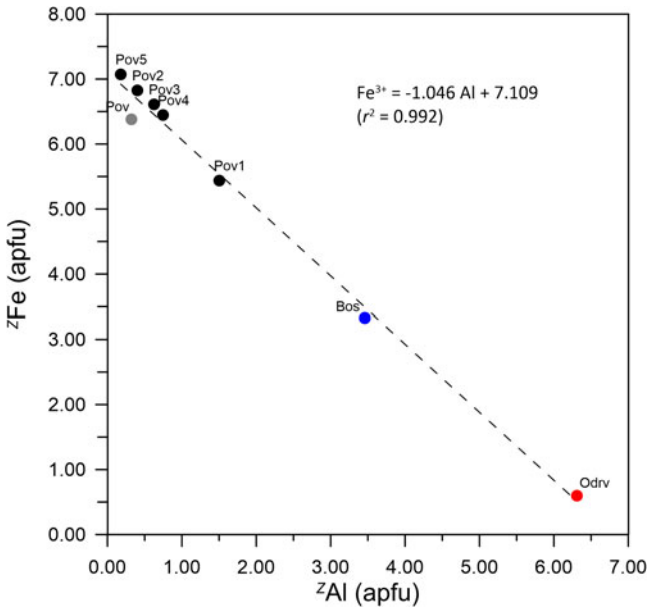

Fig. 3. Plot of Fe^{3+} *vs.* Al. The dashed black line is a linear regression based on 8 data points, which gives a slope of ~45°. Data show the occurrence of the $Fe^{3+}Al_{-1}$ substitution in the povondraite–bosiite–oxy-dravite series. Black circles represent povondraite (Pov1-5) from this study, grey circle represents povondraite (Pov) from Grice and Ercit (1993), blue circle represents bosiite (Bos) from Ertl *et al.* (2016), red circle represents oxy-dravite (Odrv) from Bosi and Skogby (2013). Abbreviations list according to Warr (2021).

whereas the band at ~3699 cm^{-1} may be caused by the arrangements $^{Y}(Fe^{3+}MgMg)$–$^{O(1)}(OH)$–$^{X}(Na,K)$.

Determination of number of atoms per formula unit (apfu)

In agreement with the structure-refinement results, the boron content was assumed to be stoichiometric (B^{3+} = 3.00 apfu). In fact, both the site-scattering results and the bond lengths of *B* and *T* are consistent with the *B* site fully occupied by B^{3+} and with the *T* site free of B^{3+} (e.g. Bosi and Lucchesi, 2007). Iron oxidation state was determined by Mössbauer spectroscopy, which shows the exclusive presence of Fe^{3+}. In accordance with Pesquera *et al.* (2016), Li concentrations were considered insignificant as MgO > 2 wt.% in the povondraite crystals studied. The (OH) content and the formula were then calculated by charge balance with the assumption (T + Y + Z) = 15 apfu and 31 anions. The excellent agreement between the number of electrons per formula unit (epfu) derived from EMPA and SREF (within 1 epfu for all studied crystals) supports the stoichiometric assumptions.

Site populations

The povondraite site populations at the *X*, *B*, *T*, O(3) (≡ V) and O(1) (≡ W) sites of crystals Pov1,2,3,4,5 follow the standard site preference suggested for tourmaline (Henry *et al.*, 2011) and are coherent with the information from FTIR absorption spectra. In particular, the presence of ~0.10 Al apfu at the *T* site is consistent with observed <*T*–O> distances ranging from 1.621–1.625 Å, which are larger than the expected value for $<^{T}Si–O> = 1.619(1)$ Å (Bosi and Lucchesi, 2007). The Fe^{3+}, Al and Mg site populations at the octahedrally coordinated *Y* and *Z* sites were optimised according to the procedure of Bosi *et al.* (2017b) and Wright *et al.* (2000), as well as by fixing the minor elements Ti^{4+} at the *Y* site. The resulting site populations are reported in Table 6, which also includes a comparison between the values of observed mean atomic number (as defined by Hawthorne *et al.*, 1995) and those calculated from the site populations. The agreement between the refined and calculated values is very good and validates the distribution of cations over the *X*, *Y*, *Z* and *T* sites in the crystals studied. This site population is also supported by the comparison of weighted bond-valence sums (BVS) and weighted atomic valence (or mean formal charge) calculated from the site populations (Table 7). It is worth noting that the presence of $^{W}(OH)$ at the O(1) site, revealed by FTIR spectra, has been quantified by using the empirical equation

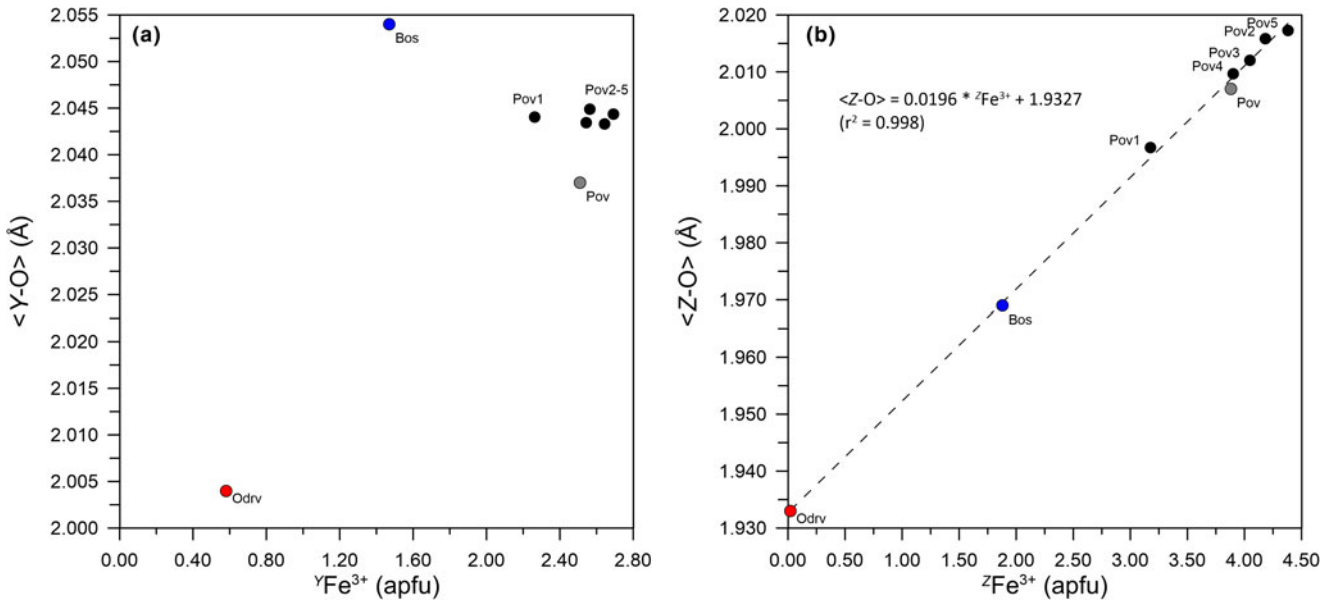

Fig. 4. Plot of <*Y*–O> *vs.* Fe^{3+} at the *Y* site (a) and plot of <*Z*–O> *vs.* Fe^{3+} at the *Z* site (b). The latter shows a much stronger correlation between the parameters than does the former. The dashed black line is a linear regression (number of data = 8 data). Sources of data as in Fig. 3.

https://doi.org/10.1180/mgm.2022.132 Published online by Cambridge University Press

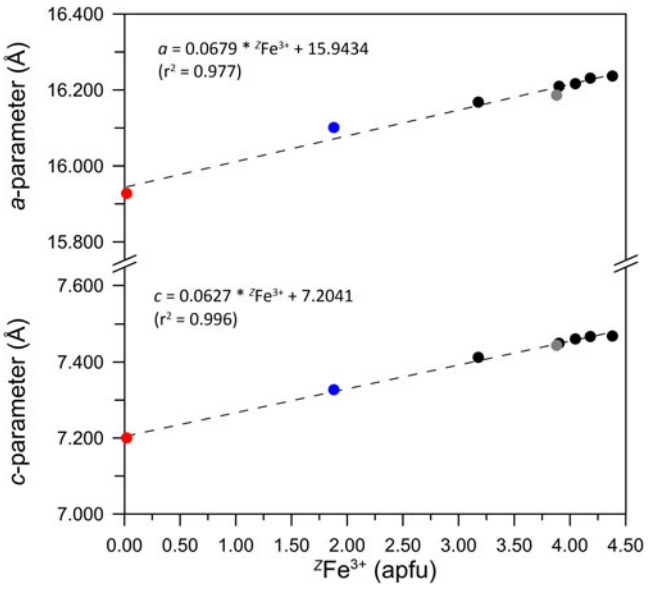

Fig. 5. Plot of *a* and *c* unit-cell parameters *vs.* Fe^{3+} at the *Z* site. The dashed black line is a linear regression (number of data = 8 data). Sources of data as in Fig. 3.

$^{W}(OH) = \{2 - [1.01 \cdot BVS(O1)] - 0.21 - F\}$ of Bosi (2013). As a result, O and (OH) are partially disordered over the O(1) and O(3) sites.

Discussion

All the crystals studied can by identified as povondraite (Table 6). More specifically, they are consistent with oxy-tourmalines belonging to the alkali group (Henry *et al.*, 2011), Na-dominant at the X position and oxy-dominant at the W position with $O^{2-} > (F + OH)$ in the tourmaline general formula. The Y position is dominated by Fe^{3+} and the Z position requires a double site-occupancy ($Fe^{3+}_4Mg_2$) for formula electroneutrality. Collectively, these constituents lead to the povondraite end-member $NaFe^{3+}_3(Fe^{3+}_4Mg_2)(Si_6O_{18})(BO_3)_3(OH)_3O$.

The five analysed crystals show a substitution series dominated by Fe^{3+} and Al, which leads to bosiite, ideally $NaFe^{3+}_3(Al_4Mg_2)(Si_6O_{18})(BO_3)_3(OH)_3O$, by the substitution $^{Z}Fe^{3+} \leftrightarrow {}^{Z}Al$, and to oxy-dravite, ideally $Na(Al_2Mg)(Al_5Mg)(Si_6O_{18})(BO_3)_3(OH)_3O$, by the substitution $^{Y}Fe^{3+}_3 + {}^{Z}Mg \leftrightarrow 2\,{}^{Y}Al_2 + {}^{Y}Mg + {}^{Z}Al$. As a result, the comprehensive substitution reaction along the povondraite–bosiite–oxy-dravite series is: $^{Y}Fe^{3+}_3 + {}^{Z}Mg + {}^{Z}Fe^{3+}_4 \leftrightarrow {}^{Y}Al_2 + {}^{Y}Mg + {}^{Z}Al_5$. The latter can be summarised as $Fe^{3+}Al_{-1}$, as shown in Fig. 3 where the substitution of Fe^{3+} for Al defines a line having a slope of ~45°. Any deviation from this line may be ascribed to other substitutional mechanisms such as coupled substitutions related to O–(OH) at the O(1) (= W) and O(3) (= V) sites. A similar $Fe^{3+}Al_{-1}$ substitution is reported in Žáček *et al.* (2000).

Sodium and K show similar variations, 0.79–0.89 apfu and 0.12–0.24 apfu, respectively, which are strongly correlated with each other (coefficient of determination, $r^2 = 0.997$) and affect the <*X*–O> mean bond-length variation (2.729–2.744 Å). In particular, the relatively high K content is related to the increase in Fe^{3+} (Table 4). As noted by Bačík *et al.* (2008), the incorporation of a relatively large cation such as K (+ Na) into the povondraite structure should be favoured by the larger unit-cell of Fe^{3+} – relative to Al-dominant tourmalines such as bosiite or oxy-dravite (see below). This mechanism is different from that involved in maruyamaite (K- and Al-dominant tourmaline) in which the

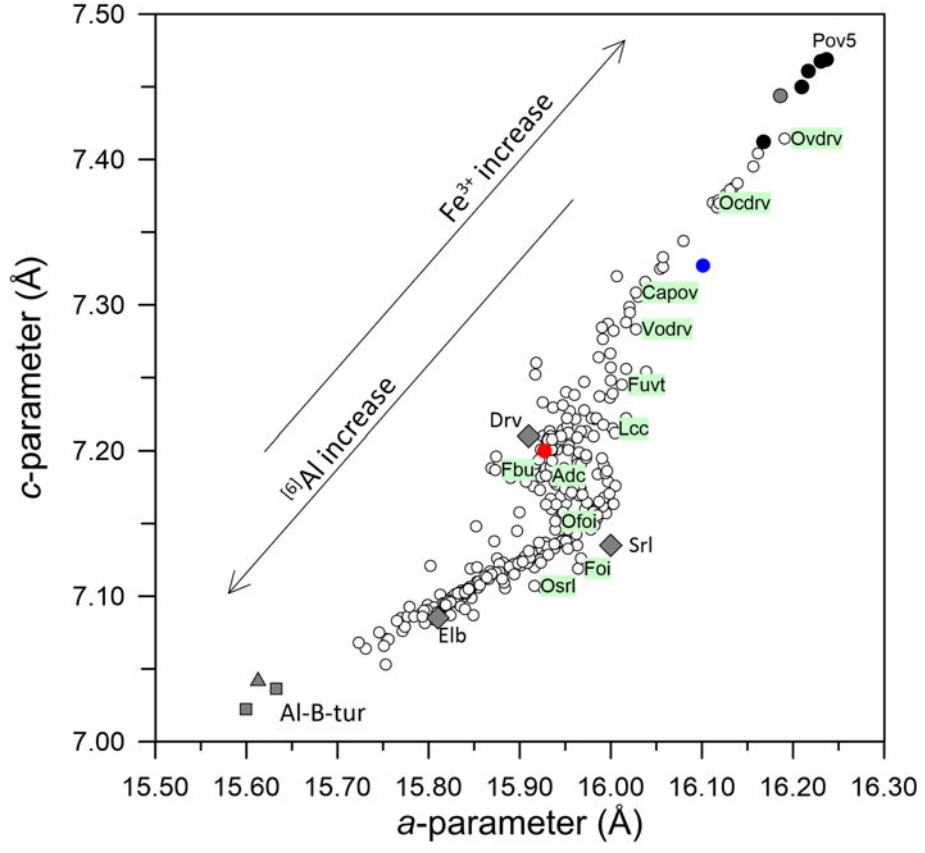

Fig. 6. Plot of *a* against *c* showing the whole variation of the unit-cell parameters in the tourmaline-supergroup minerals. Plot obtained using 326 data sets with structure refinement. In detail, black circles represent povondraite from this study, a grey circle represents povondraite from Grice and Ercit (1993), a blue circle represents bosiite from Ertl *et al.* (2016), a red circle represents oxy-dravite from Bosi and Skogby (2013), white circles represent data from literature (see figure 3 of Bosi, 2018), grey squares represent samples from Marler *et al.* (2002), a grey triangle symbol represents samples from Kutzschbach *et al.* (2016), and grey diamonds represent the ideal value from Epprecht (1953). Text symbols: Elb = elbaite, Drv = dravite, Srl = schorl. Text symbols highlighted in pale green refer to holotypes data of $^{Y}(Fe^{2+},Fe^{3+})$, Cr- and V-dominant tourmalines: Ovdrv = oxy-vanadium-dravite (Bosi *et al.*, 2013), Ocdrv = oxy-chromium-dravite (representing also vanadio-chromium-oxy-dravite; Bosi *et al.*, 2012, 2014a), Capov = chromo-alumino-povondraite (Reznitskii *et al.*, 2014), Vodv = Vanadio-oxy-dravite (Bosi *et al.*, 2014b), Lcc = lucchesiite (Bosi *et al.*, 2017a), Fbu = fluor-buergerite (Donnay *et al.*, 1966), Adc = Adachiite (Nishio-Hamane *et al.*, 2014), Ofoi = oxy-foitite (Bosi *et al.*, 2017c), Foi = foitite (MacDonald *et al.*, 1993), Osrl = oxy-schorl (Bačík *et al.*, 2013). Abbreviations list according to Warr (2021).

https://doi.org/10.1180/mgm.2022.132 Published online by Cambridge University Press

substitution K → Na occurs only under high-pressure conditions (Berryman *et al.*, 2014; Lussier, *et al.*, 2016).

As for the octahedrally coordinated cations, Mg varies from 1.84 to 2.02 apfu and occupies both the *Y* and *Z* sites, whereas Al varies from 0.18 to 1.50 apfu and is ordered at the *Z* site. Ferric iron varies from 5.44 to 7.07 apfu, showing a rather disordered distribution over the *Y* and *Z* sites.

Despite the significant $^{Y}Fe^{3+}$ variations in the present povondraite crystals, the <*Y*–O> values are practically constant; the increase in contents of the smaller cation $^{Y}Fe^{3+}$ (2.26–2.69 apfu), accompanied by decrease in contents of the larger cation ^{Y}Mg (0.31–0.66 apfu), do not produce any decrease in <*Y*–O> (2.043–2.045 Å). Therefore, we may infer that the accommodation of Fe at the *Y* site should produce a <*Y*–O> expansion that compensates for the differences in size between Fe^{3+} and Mg^{2+} substituent ions. This expansion may be shown by the smaller values of bond-valence sum at *Y* (2.69–2.74 vu) with respect to the weighted atomic valence at *Y* (2.81–2.90 vu) (Table 7), indicating that the Y-cation is underbonded and bond lengths in the YO_6 polyhedron are stretched (Bosi, 2014).

In general, the variation of the structural parameters is dominated by Fe^{3+} (or Al). No significant correlation occurs between <*Y*–O> and $^{Y}Fe^{3+}$ (Fig. 4a), whereas the <*Z*–O> variation (1.997–2.017 Å) is positively correlated with $^{Z}Fe^{3+}$ (Fig. 4b) and negatively correlated with ^{Z}Al (not shown; $r^2 = 0.98$). Similarly, the *a*- and *c*-parameter are positively related to $^{Z}Fe^{3+}$ (Fig. 5).

The *a*- and *c*-parameters show similar variations in the studied crystals, 16.1679(2)–16.2366(3) Å and 7.4122(1)–7.4688(2) Å, respectively, which are positively correlated ($r^2 = 0.98$). Povondraite has relatively large unit-cell parameters with respect to other tourmalines due to the larger size of Fe^{3+} compared to other trivalent cations $V^{3+} > Cr^{3+} > Al^{3+}$ (Bosi, 2018). The plot of *a* against *c* (Fig. 6) shows the variation of these parameters in the tourmaline-supergroup minerals (*a* range ~15.60–16.25 Å and *c* range ~7.00–7.50 Å) and their increase with increasing Fe^{3+} or decreasing Al. In particular, the smallest *a*- and *c*-parameters are those of synthetic Al-B-tourmalines, whose compositions lead to the end-members $NaAl_3Al_6(Si_3B_3O_{18})(BO_3)_3(OH)_3(OH)$ (Schreyer *et al.*, 2000; Marler *et al.*, 2002) and $NaAl_3Al_6(Si_4B_2O_{18})(BO_3)_3(OH)_3O$ (Kutzschbach *et al.*, 2016), whereas the largest ones are of povondraite crystal pov5 of the present study.

Acknowledgements. The authors are grateful to George E. Harlow (American Museum of Natural History, New York, USA) for kindly furnishing povondraite sample 110379 to G.H. (Hovis *et al.*, in press) along with well wishes for the further study reported here. Chemical analyses were done with the kind assistance of Beatrice Celata to whom the authors express their gratitude. Comments by the Structural Editor (P. Leverett) and reviewers Peter Bačík and Darrell Henry are very much appreciated. F.B. acknowledges funding by Sapienza University of Rome (Prog. Università 2020) and by the Italian Ministry of Education (MIUR)–PRIN 2020, ref. 2020WYL4NY.

Supplementary material. To view supplementary material for this article, please visit https://doi.org/10.1180/mgm.2022.132

Competing interests. The authors declare none.

References

Bačík P. and Fridrichová G. (2020) Cation partitioning among crystallographic sites based on bond-length constraints in tourmaline-supergroup minerals. *American Mineralogist*, **106**, 851–861, https://doi.org/10.2138/am-2021-7804.

Bačík P., Uher P., Sykora M. and Lipka J. (2008) Low-Al tourmalines of the schorl – dravite – povondraite series in redeposited tourmalinites from the Western Carpathians, Slovakia. *The Canadian Mineralogist*, **46**, 1117–1129.

Bačík P., Cempírek J., Uher P., Novák M., Ozdín D., Filip J., Škoda R., Breiter K., Klementová M. and Ďuďa R. (2013) Oxy-schorl, Na(Fe22+Al) Al6Si6O18 (BO3)3(OH)3O, a new mineral from Zlatá Idka, Slovak Republic and Prˇibyslavice, Czech Republic. *American Mineralogist*, **98**, 485–492.

Berryman E., Wunder B. and Rhede D. (2014) Synthesis of K-dominant tourmaline. *American Mineralogist*, **99**, 539–542.

Bosi F. (2013) Bond-valence constraints around the O1 site of tourmaline. *Mineralogical Magazine*, **77**, 343–351.

Bosi F. (2014) Mean bond-length variation in crystal structures: A bond-valence approach. *Acta Crystallographica*, **B70**, 697–704.

Bosi F. (2018) Tourmaline crystal chemistry. *American Mineralogist*, **103**, 298–306.

Bosi F. and Lucchesi S. (2007) Crystal chemical relationships in the tourmaline group: structural constraints on chemical variability. *American Mineralogist*, **92**, 1054–1063.

Bosi F. and Skogby H. (2013) Oxy-dravite, $Na(Al_2Mg)(Al_5Mg)(Si_6O_{18})(BO_3)_3(OH)_3O$, a new mineral species of the tourmaline supergroup. *American Mineralogist*, **98**, 1442–1448.

Bosi F., Reznitskii L. and Skogby H. (2012) Oxy-chromium-dravite, $NaCr_3(Cr_4Mg_2)(Si_6O_{18})(BO_3)_3(OH)_3O$, a new mineral species of the tourmaline supergroup. *American Mineralogist*, **97**, 2024–2030.

Bosi F., Reznitskii L. and Sklyarov E.V. (2013) Oxy-vanadium-dravite, $NaV_3(V_4Mg_2)(Si_6O_{18})(BO_3)_3(OH)_3O$: crystal structure and redefinition of the "vanadium-dravite" tourmaline. *American Mineralogist*, **98**, 501–505.

Bosi F., Reznitskii L., Skogby H. and Hålenius U. (2014a) Vanadio-oxy-chromium-dravite, $NaV_3(Cr_4Mg_2)(Si_6O_{18})(BO_3)_3(OH)_3O$, a new mineral species of the tourmaline supergroup. *American Mineralogist*, **99**, 1155–1162.

Bosi F., Skogby H., Reznitskii L. and Hålenius U. (2014b) Vanadio-oxy-dravite, $NaV_3(Al_4Mg_2)(Si_6O_{18})(BO_3)_3(OH)_3O$, a new mineral species of the tourmaline supergroup. *American Mineralogist*, **99**, 218–224.

Bosi F., Skogby H., Lazor P. and Reznitskii L. (2015) Atomic arrangements around the O3 site in Al- and Cr-rich oxy-tourmalines: a combined EMP, SREF, FTIR and Raman study. *Physics and Chemistry of Minerals*, **42**, 441–453.

Bosi F., Skogby H. and Balić-Žunić T. (2016) Thermal stability of extended clusters in dravite: a combined EMP, SREF and FTIR study. *Physics and Chemistry of Minerals*, **43**, 395–407.

Bosi F., Skogby H., Ciriotti M.E., Gadas P., Novák M., Cempírek J., Všianský D. and Filip J. (2017a) Lucchesiite, $CaFe^{2+}_3Al_6(Si_6O_{18})(BO_3)_3(OH)_3O$, a new mineral species of the tourmaline supergroup. *Mineralogical Magazine*, **81**, 1–14.

Bosi F., Reznitskii L., Hålenius U. and Skogby H. (2017b) Crystal chemistry of Al–V–Cr oxy-tourmalines from Sludyanka complex, Lake Baikal, Russia. *European Journal of Mineralogy*, **29**, 457–472.

Bosi F., Skogby H. and Hålenius U. (2017c) Oxy-foitite, $□(Fe^{2+}Al_2)Al_6(Si_6O_{18})(BO_3)_3(OH)_3O$, a new mineral species of the tourmaline supergroup. *European Journal of Mineralogy*, **29**, 889–896.

Cempírek J., Houzar S., Novák M., Groat L.A., Selway J.B. and Šrein V. (2013) Crystal structure and compositional evolution of vanadium-rich oxy-dravite from graphite quartzite at Bítovánky, Czech Republic. *Journal of Geosciences*, **58**, 149–162.

Donnay G., Ingamells C.O. and Mason B.H. (1966) Buergerite, a new species of tourmaline. *American Mineralogist*, **50**, 198–199.

Epprecht W. (1953) Die Gitterkonstanten der Turmaline. Schweizerische *Mineralogische und Petrographische Mitteilungen*, **33**, 481–505.

Ertl A., Hughes J.M., Pertlik F., Foit F.F. Jr., Wright S.E., Brandstatter F. and Marler B. (2002) Polyhedron distortions in tourmaline. *The Canadian Mineralogist*, **40**, 153–162.

Ertl A., Baksheev I.A., Giester G., Lengauer C.L., Prokofiev V.Yu. and Zorina L.D. (2016) Bosiite, $NaFe^{+3}_3(Al_4Mg_2)(Si_6O_{18})(BO_3)_3(OH)_3O$, a new ferric member of the tourmaline supergroup from the Darasun gold deposit, Transbaikalia, Russia. *European Journal of Mineralogy*, **28**, 581–591.

Foit F.F. Jr. (1989) Crystal chemistry of alkali-deficient schorl and tourmaline structural relationships. *American Mineralogist*, **74**, 422–431.

Gagné O.C. and Hawthorne F.C. (2015) Comprehensive derivation of bond-valence parameters for ion pairs involving oxygen. *Acta Crystallographica*, **B71**, 562–578.

Gatta G.D., Bosi F., McIntyre G.J. and Skogby H. (2014) First accurate location of two proton sites in tourmaline: A single-crystal neutron diffraction study of oxy-dravite. *Mineralogical Magazine*, **78**, 681–692.

Gonzales-Carreño T., Fernández M. and Sanz J. (1988) Infrared and electron microprobe analysis of tourmaline. *Physics and Chemistry of Minerals*, **15**, 452–460.

Grice J.D. and Ercit T.S. (1993) Ordering of Fe and Mg in the tourmaline crystal structure: the correct formula. *Neues Jahrbuch für Mineralogie, Abhandlungen*, **165**, 245–266.

Grice J.D., Ercit T.S. and Hawthorne F.C. (1993) Povondraite, a redefinition of the tourmaline ferridravite. *American Mineralogist*, **78**, 433–436.

Hawthorne F.C. and Henry D. (1999) Classification of the minerals of the tourmaline group. *European Journal of Mineralogy*, **11**, 201–215.

Hawthorne F.C., Ungaretti L. and Oberti R. (1995) Site populations in minerals: terminology and presentation of results of crystal-structure refinement. *The Canadian Mineralogist*, **33**, 907–911.

Henry D.J. and Dutrow B.L. (2011) The incorporation of fluorine in tourmaline: Internal crystallographic controls or external environmental influences? *Canadian Mineralogist*, **49**, 41–56.

Henry D.J., Novák M., Hawthorne F.C., Ertl A., Dutrow B., Uher P. and Pezzotta F. (2011) Nomenclature of the tourmaline supergroup minerals. *American Mineralogist*, **96**, 895–913.

Hovis G.L., Tribaudino M., Altomare C. and Bosi F. (in press) Thermal expansion of minerals in the tourmaline supergroup. *American Mineralogist*, doi.org/10.2138/am-2022-8580.

Kutzschbach M., Wunder B., Rhede D., Koch-Mueller M., Ertl A., Giester G., Heinrich W. and Franz G. (2016) Tetrahedral boron in natural and synthetic HP/UHP tourmaline: Evidence from Raman spectroscopy, EMPA, and single crystal XRD. *American Mineralogist*, **101**, 93–104.

Levy E.A., Henry D.J., Roy A. and Dutrow B.L. (2018) Determination of ferrous-ferric iron contents in tourmaline using synchrotron-based XANES. *Journal of Geosciences*, **63**, 167–174.

Lussier A.J., Ball N.A., Hawthorne F.C., Henry D.J., Shimizu R., Ogasawara Y. and Ota T. (2016) Maruyamaite, $K(MgAl_2)(Al_5Mg)Si_6O_{18}(BO_3)_3(OH)_3O$, from the ultrahigh-pressure Kokchetav massif, northern Kazakhstan: Description and crystal structure. *American Mineralogist*, **101**, 355–361.

MacDonald D.J., Hawthorne F.C. and Grice J.D. (1993) Foitite, $\square[Fe^{2+}_2(Al,Fe^{3+})]Al_6Si_6O_{18}(BO_3)_3(OH)_4$, a new alkali-deficient tourmaline: Description and crystal structure. *American Mineralogist*, **78**, 1299–1303.

Marler B., Borowski M., Wodara U. and Schreyer W. (2002) Synthetic tourmaline (olenite) with excess boron replacing silicon in the tetrahedral site: II. Structure analysis. *European Journal of Mineralogy*, **14**, 763–771.

Nishio-Hamane D., Minakawa T., Yamaura J., Oyama T., Ohnishi M. and Shimobayashi N. (2014) Adachiite, a Si–poor member of the tourmaline supergroup from the Kiura mine, Oita Prefecture, Japan. *Journal of Mineralogical and Petrological Sciences*, **109**, 74–78.

Novák M., Povondra P. and Selway J.B. (2004) Schorl-oxy-schorl to dravite-oxydravite tourmaline from granitic pegmatites; examples from the Moldanubicum, Czech Republic. *European Journal of Mineralogy*, **16**, 323–333.

Pesquera A., Gil-Crespo P.P Torres-Ruiz F., Torres-Ruiz J. and Roda-Robles E. (2016) A multiple regression method for estimating Li in tourmaline from electron microprobe analyses. *Mineralogical Magazine*, **80**, 1129–1133.

Pouchou J.L. and Pichoir F. (1991) Quantitative analysis of homogeneous or stratified microvolumes applying the model "PAP." Pp. 31–75 in: Electron Probe Quantitation (K.F.J. Heinrich and D.E. Newbury, editors). Plenum, New York.

Prescher C., McCammon C. and Dubrowinsky L. (2012) *MossA*: a program for analyzing energy-domain Mössbauer spectra from conventional and synchrotron sources. *Journal of Applied Crystallography*, **45**, 329–331.

Reznitskii L., Clark C.M., Hawthorne F.C., Grice J.D., Skogby H., Hålenius U. and Bosi F. (2014) Chromo-alumino-povondraite, $NaCr_3(Al_4Mg_2)(Si_6O_{18})(BO_3)_3(OH)_3O$, a new mineral species of the tourmaline supergroup. *American Mineralogist*, **99**, 1767–1773.

Schreyer W., Wodara U., Marler B., van Aken P.A., Seifert F. and Robert J.L. (2000) Synthetic tourmaline (olenite) with excess boron replacing silicon in the tetrahedral site: I. Synthesis conditions, chemical and spectroscopic evidence. *European Journal of Mineralogy*, **12**, 529–541.

Sheldrick G.M. (2015) Crystal structure refinement with SHELXL. *Acta Crystallographica*, **C71**, 3–8.

Walenta K. and Dunn P.J. (1979) Ferridravite, a new mineral of the tourmaline group from Bolivia. *American Mineralogist*, **64**, 945–948.

Warr L.N. (2021) IMA–CNMNC approved mineral symbols. *Mineralogical Magazine*, **85**, 291–320.

Watenphul A., Burgdorf M., Schlüter J., Horn I., Malcherek T. and Mihailova B. (2016) Exploring the potential of Raman spectroscopy for crystallochemical analyses of complex hydrous silicates: II. Tourmalines. *American Mineralogist*, **101**, 970–985.

Wright S.E., Foley J.A. and Hughes J.M. (2000) Optimization of site occupancies in minerals using quadratic programming. *American Mineralogist*, **85**, 524–531.

Žáček V., Frýda J., Petrov A. and Hyršl J. (2000) Tourmalines of the povondraite—(oxy)dravite series from the caps rocks of meta-evaporite in Alto Chapare, Cochamba, Bolivia. *Journal of the Czech Geological Society*, **45**, 3–12.

https://doi.org/10.1180/mgm.2022.132 Published online by Cambridge University Press